J Mater Sci (2009) 44:212–220
DOI 10.1007/s10853-008-3096-x

Cyclic hardening behavior for interstitial-free steel

Chia-Chang Shih · New-Jin Ho · Hsing-Lu Huang

Received: 4 August 2008 / Accepted: 29 October 2008 / Published online: 27 November 2008

Abstract Strain-controlled fatigue experiments were employed to evaluate automotive-grade interstitial-free ferrite steels under $R = 0$. Hundreds of grains were examined by scanning electron microscope (SEM) under electron channeling contrast image technique of backscattered electron image mode (BEI/ECCI) for comprehensive comparison of micrographs with those taken under transmission electron microscope (TEM). It is clearly revealed that cyclic hardening was virtually unobvious and dislocation cell structures were very rare when $\Delta\varepsilon/2$ was controlled to within 0.1%. When $\Delta\varepsilon/2$ was increased to 0.2%, the general dislocation structure exhibited a predominately dislocation wall structure prior to the secondary cyclic hardening, after which the formation of dislocation cells were observed. At $\Delta\varepsilon/2 = 1.0\%$, following an initial rapid-hardening stage, the dislocation cell structure of low-angle misorientation formed in the early stage was gradually converted into high-angle misorientation as the cyclic strain continued to be imposed.

Introduction

It is generally accepted that microstructural change is accompanied by a cyclic hardening curve, and that well-annealed pure face-centered cubic (FCC) metals subjected to cyclic deformation at constant plastic strain amplitudes exhibit an initial rapid hardening stage, followed by a regime of cyclic saturation and, finally, suffer from fatigue failure [1–8]. However there are some reports in the literature on fatigued FCC metals, including aluminum [4, 6–13], with a secondary hardening prior to failure at some plastic strain amplitudes, which is attributed to the appearance of a dislocation cell structure. By comparison, fatigued body-centered cubic (BCC) metals have received less attention concerning the fundamental fatigue mechanisms. With regard to the cyclic hardening behavior for fatigued BCC metals, much of the literature has either merely paid attention to the early and saturated stage of cyclic deformation [14–20] or outrightly ignored the secondary cyclic hardening [5, 21], except for the studies of Abdel-Raouf et al. [22], Chopra et al. [23], and Ikeda [24]. Nevertheless, Abdel-Raouf et al., Chopra et al., and Ikeda have never systematically studied and interpreted the cyclic hardening behaviors from the perspectives of dislocation gliding and subsequent dislocation development, thus leaving the correlation between dislocation structures and secondary cyclic hardening behaviors for fatigued BCC metals largely in the uncharted territory. Furthermore, with regard to IF steel and α-iron, the dislocation cell size has been reported to be in direct proportion to the shear modulus [25, 26], while the shear moduli of IF steel and α-iron are about twice as high as that of copper. Hence the sizes of dislocation cells and the relevant characteristics may be different from copper, possibly resulting in dissimilar cyclic hardening behaviors.

Previously, the microstructures of fatigued metals have been observed using TEM. However, due to the very limited spatial regions that could be used to observe the dislocation structures, this experiment will utilize a SEM to supplement the TEM. Recently the BEI/ECCI mode has

C.-C. Shih · N.-J. Ho
Institute of Materials Science and Engineering, National Sun Yat-Sen University, Kaohsiung, Taiwan, ROC

H.-L. Huang (✉)
Department of Mechanical Engineering, Chinese Military Academy, Kaohsiung, Taiwan, ROC
e-mail: hlhuang8423@gmail.com

received much interest for studying dislocation configurations in deformed materials [27–33]. Dislocation morphologies can be more extensively examined by SEM under the BEI/ECCI mode, which allows for more than 100 grains to be observed simultaneously because of the larger observable area. Under the assistance of the BEI/ECCI mode, this study attempts to clarify the role that dislocation development plays during the secondary cyclic hardening stage for fatigued IF steel, and to understand the hardening mechanisms underlying different cyclic hardening curves in fatigue tests for the BCC metals.

Experimental

A hot rolled polycrystalline interstitial-free steel (IF steel) plate with a chemical composition of C <50 ppm, N <50 ppm, S <120 ppm, B ≈2 ppm, Mn ≈0.15 wt%, Ti ≈0.04 wt%, and balance Fe was used in this study. The material was annealed at 800 °C for 2 h and then cooled in a furnace to obtain an average grain size of about 80 μm in diameter. The preparation of specimens followed the ASTM E606 specification. A computerized Instron 8801 hydraulic testing machine was employed at a testing strain rate of 4×10^{-3} s^{-1} with $R = 0$ at room temperature. The tests on IF steels were performed with total strain amplitudes ($\Delta\varepsilon/2$) ranging from 0.1% to 1.0%. The marks I1 to K2 shown in Fig. 1 denote the samples to be by TEM or SEM. The strain amplitudes were 0.1, 0.2, and 1.0% for samples numbered as In, Jn, and Kn, respectively. All fatigued samples were cut into slices of 1 mm thickness. The slices were ground to a thickness about of 0.3 mm for SEM and 0.1 mm for TEM observations using abrasive paper and punched into 3 mm-diameter disks. The 3 mm disks were twin-jet polished using a solution of 90% methanol diluted with 10% perchlorate at 15 V and −40 °C. For microstructure observations, a Philips Quant200 SEM under BEI mode was used to obtain electron channeling contrast images (ECCI), and a Philips CM200 TEM under bright field image (BFI) and two beam modes were employed to obtain higher-resolution images.

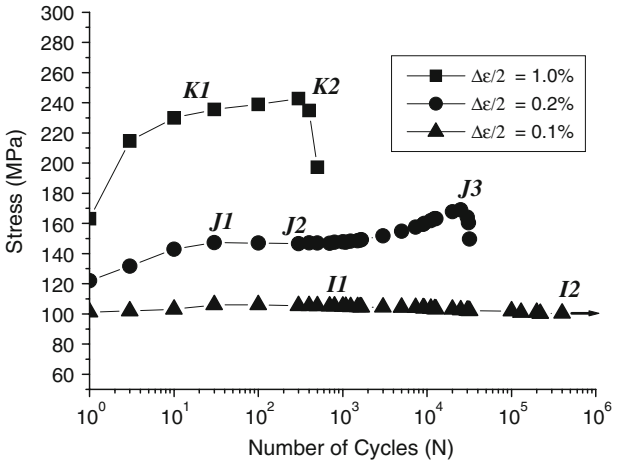

Fig. 1 The curve of stress versus number of cycles in low cycle fatigue at various strain amplitudes. The marks I1 to K2 denote samples observed by TEM or SEM

Results and discussion

The relation of cyclic responding stress versus the number of cycles shown in Fig. 1 clearly demonstrates that fatigue failure would not occur if the strain amplitude is controlled at $\Delta\varepsilon/2 = 0.1\%$, since no significant cyclic hardening has taken place. When the strain amplitude is increased to $\Delta\varepsilon/2 = 0.2\%$, the cyclic responding stress rapidly increases to about 150 MPa in the early stage of cycling, which then tends to saturate, after which a secondary hardening begins to occur at about 3,000 cycles and continues to harden till failure. As for $\Delta\varepsilon/2 = 1.0\%$, the cyclic hardening curve tends to flatten out after a rapid (primary) hardening, with the stress increasing slightly thereafter for further cyclic deformation. In contrast with $\Delta\varepsilon/2 = 0.2\%$, here no secondary hardening was observable prior to fatigue failure.

Exact identification of the dislocations in loop patches/veins was performed by the double-tilting technique in the TEM. Figure 2 shows the loop patch structure is the corresponding dislocation structure for strain amplitude controlled at $\Delta\varepsilon/2 = 0.1\%$ and cycled to 1,000 cycles (sample I1). It can be seen that the dislocations in those loop patches are visible when g = [01−1] and [1−10] at B ≈ [111], while significantly reduced in contrast when g = [10−1] at B ≈ [111]. Moreover, there are many dislocations gliding freely between the loop patches and they are almost perpendicular to the loop patches. These dislocations are invisible when g = [10−1] at B ≈ [111], identifying them as screw dislocations with the primary Burgers vector of [1−11].

The ability to examine hundreds of grains by SEM under BEI/ECCI mode allows one to compare it with the observation under TEM/BFI. The dislocation structures after 4×10^5 cycles at $\Delta\varepsilon/2 = 0.1\%$ (sample I2), as shown in Fig. 3a, are mainly composed of loop patches/veins, though, in addition, a few dislocation cells also can be found. Figure 3b is a high-magnification observation of the mark M in Fig. 3a, and Fig. 3c–e are the similar morphologies shown in TEM for comparison where the loop patches/veins are significantly reduced in contrast when g = [01−1] at B ≈ [111]. The morphologies shown in Fig. 3c–e tend to be oriented along the same direction with no contrast caused by misorientation. This implies that the loop patches/veins shown in Fig. 3c–e are only composed

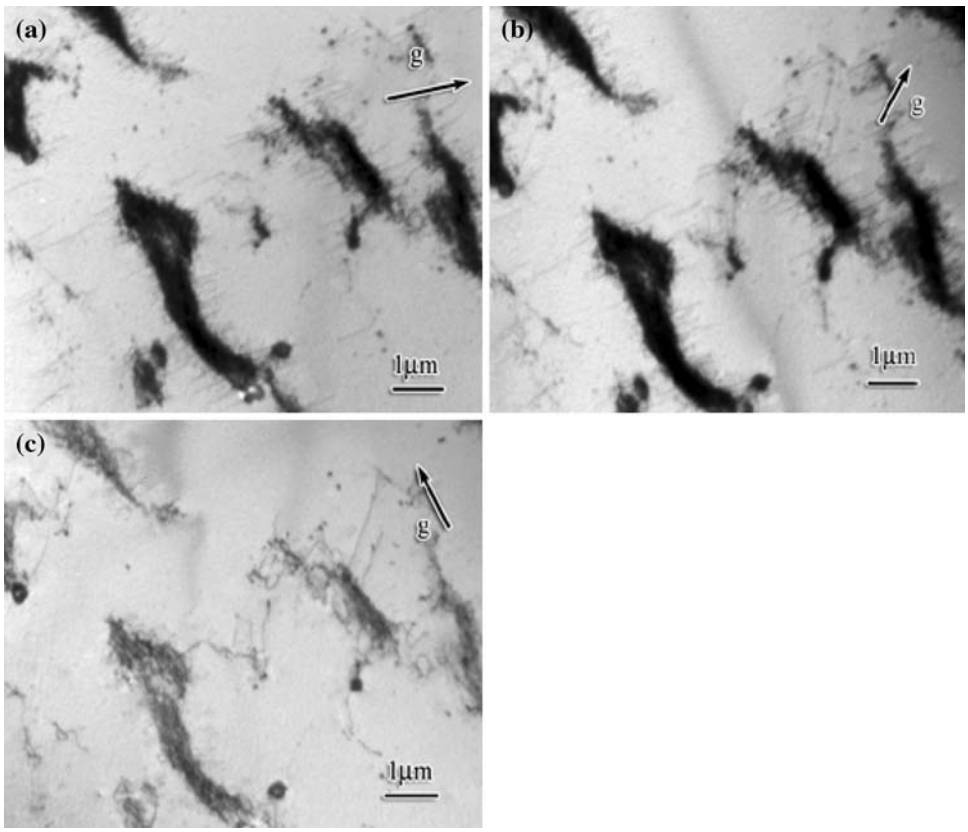

Fig. 2 Microstructure of IF steel cyclically deformed at $\Delta\varepsilon/2 = 0.1\%$ and cycled to 1000 cycles (sample I1) where TEM micrographics show the analyses of the loop patches under three g vectors: **a** B $\approx$ [111], g = [01−1]; **b** B $\approx$ [111], g = [1−10]; and **c** B $\approx$ [111], g = [10−1]

of a primary Burgers vector of [−111]. Therefore, the gliding behavior of dislocations for $\Delta\varepsilon/2 = 0.1\%$ from early stage to 4×10^5 cycles is a single slip principally. Figure 3e is high-magnification observation of the mark N in Fig. 3a, where it can be seen that all these dislocation cells are larger than 2 μm. Although these dislocation cells reveal misorientation, there is almost no cyclic hardening or any occurrence of fatigue failure in this fatigue condition. Consequently, for $\Delta\varepsilon/2 = 0.1\%$, it can be concluded that no corresponding dislocation structures contribute to the cyclic hardening as they cannot impede the dislocation gliding efficiently during the time, and thus would not induce fatigue failure.

Figure 4b displays a high-magnification observation of the mark Q in Fig. 4a, which shows that the dislocation wall structure predominates the microstructure after 30 cycles at $\Delta\varepsilon/2 = 0.2\%$ (sample J1), suggesting that the dislocation walls had already been formed in the early stages of cyclic deformation. There are no dislocation walls out of contrast under three g vectors as shown in Fig. 4d–f. This implies that these dislocation walls in Fig. 4d–f contain at least two kinds of Burgers vector. In the channels of the dislocation wall structure, some gliding dislocations are invisible when g = [01−1] at B $\approx$ [111], while others are invisible when g = [10−1] at B $\approx$ [111]. Since they all are almost perpendicular to respective diffraction g vectors with $g \cdot b = 0$, they are mainly screw in character with Burgers vectors of [−111] (Mark B1 in Fig. 4e) and [1−11] (Mark B2 in Fig. 4e), respectively. Based on above analyses, those dislocation walls are formed by these two kinds of Burgers vector cooperatively. In other words, the two Burgers vectors can start simultaneously when the strain amplitude is controlled at $\Delta\varepsilon/2 = 0.2\%$, and this can be treated as a double slip. Moreover, the average dislocation wall orientation at $\Delta\varepsilon/2 = 0.2\%$ is not perpendicular to either Burgers vectors. Hence, the gliding direction of these dislocations is not parallel to the orientation of any dislocation walls, thus keeping the dislocation gliding restrained to some extent. Therefore, the gliding of screw dislocations at $\Delta\varepsilon/2 = 0.2\%$ is not so smooth as in the case of $\Delta\varepsilon/2 = 0.1\%$. This is one of the causes for the occurrence of primary (rapid) cyclic hardening at $\Delta\varepsilon/2 = 0.2\%$.

Figure 5 shows that the dislocation wall structure is still predominant in the microstructure, which is consistent with the cyclic hardening curve due to the close similarity between the corresponding cyclic stress of samples J1 and J2. Figures 4a, 5a both reveal almost no contrast within the grains, which means that the dislocation arrangement has been unable to create a misoriented cell structure. Figure 5d is the high-magnification observation of the mark S in Fig. 5c, showing the same behavior of dislocation gliding as in sample J1 where there are many dislocations of two different Burgers vectors (as mark B1 and B2, where Burgers vectors of B1 = [−111], B2 = [1−11]) are gliding in

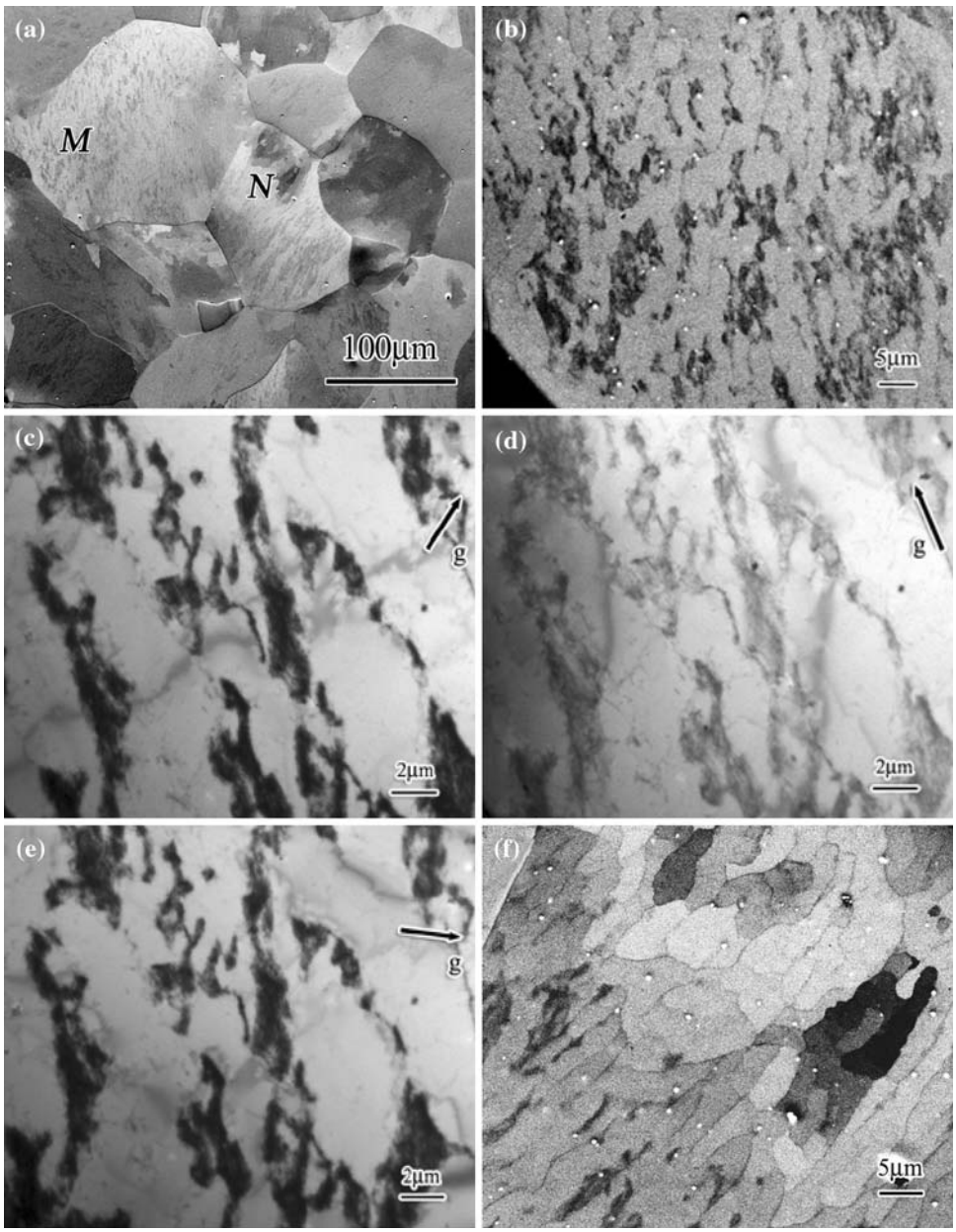

Fig. 3 Microstructure of IF steel cyclically deformed at $\Delta\varepsilon/2 = 0.1\%$ and cycled to 4×10^5 cycles without failure (sample I2): **a** SEM micrograph under BEI/ECCI mode showing loop patches/veins (mark M) developed within most of grains, and only a few large dislocation cells (mark N) developed near grain boundary; **b** mark M in (**a**) showing detailed loop patches/veins morphologies; **c** similar morphologies shown in TEM/BFI for comparison, where B $\approx$ [111], g = [1−10]; and **d** B $\approx$ [111], g = [01−1]; **e** B $\approx$ [111], g = [10−1]; **f** mark N in (**a**)

the channels of the dislocation wall structure simultaneously. Therefore the dislocation wall that we observed also cannot obstruct the dislocation gliding completely, and that can explain why the cyclic stress remains constant at a stage between primary and secondary hardening.

Compared with samples J1 and J2, sample J3 ($\Delta\varepsilon/2 = 0.2\%$ and cycled to failure) shows an extreme difference in dislocation structure as judged from the contrast variety inside the grains under the BEI/ECCI mode shown in Fig. 6a, where the corresponding structure is from the dislocation cells. Figure 6b is a high-magnification observation of the mark U in Fig. 6a, and Fig. 6c shows the similar morphologies in TEM/BFI for comparison, where these dislocation cells are smaller than 2 μm and their cell boundaries are very condensed. Moreover, the interior of the dislocation cells are free of dislocation. This suggests that the dislocation structures have transformed into dislocation cells from the dislocation wall structure during the secondary cyclic hardening, and also implies that the gliding dislocations have been restrained by the dislocation cells. The formation of dislocation cells may enable the secondary cyclic hardening to occur and thus requires a higher stress to accommodate the applied plastic strain. Therefore the secondary cyclic hardening will certainly be accompanied by the accumulation of cyclic strain when the cyclic strain is controlled at $\Delta\varepsilon/2 = 0.2\%$.

On the other extreme, namely at very large strain amplitudes such as $\Delta\varepsilon/2 = 1.0\%$, the dislocation cells with

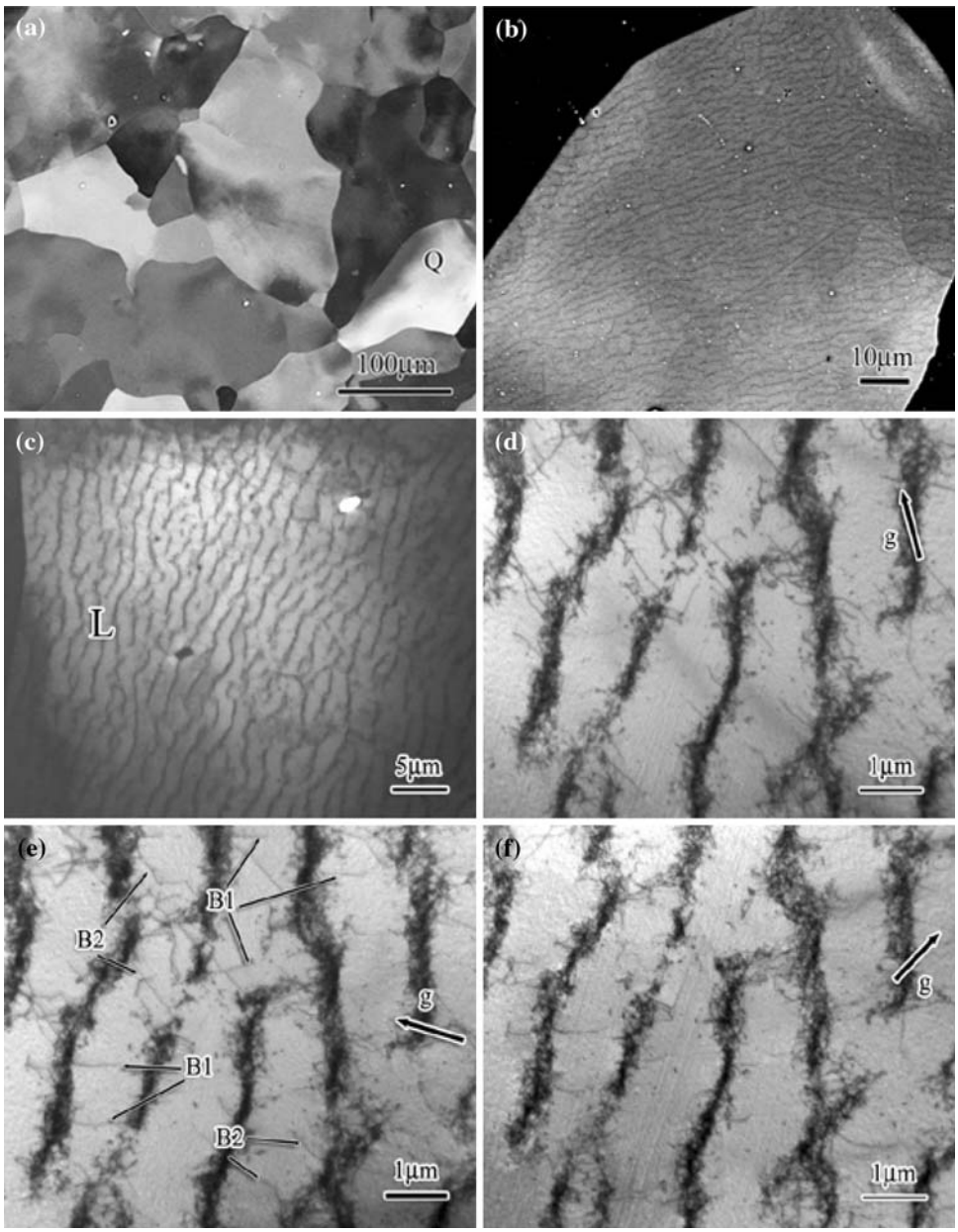

Fig. 4 Microstructure of IF steel cyclically deformed at $\Delta\varepsilon/2 = 0.2\%$ and cycled to 30 cycles without failure (sample J1): **a** SEM micrograph under BEI/ECCI mode showing no contrast within the grains, this represents there is no misorientation in all grains; **b** mark Q in (**a**) showing detailed dislocation wall structure; **c** similar morphologies shown in TEM/BFI for comparison; **d** mark L in (**c**) where B $\approx$ [111], g = [01−1]; **e** mark L in (**c**) where B $\approx$ [111], g = [1−10]; **f** mark L in (**c**) where B $\approx$ [111], g = [10−1]

low-angle misorientation originate from multislip in the early stage of cyclic deformation (sample K1), as shown in Fig. 7, and are gradually converted into high-angle misorientation when accompanied by an accumulation of cyclic strain before failure, as shown in Fig. 8 (sample K2). This finding is consistent with previous investigations [19, 23, 24] which studied the cyclically deformed α-Fe monocrystals and polycrystals and reported that the dislocation cell walls became progressively sharper and more condensed in saturation, accompanied by increasing misorientation, hence causing the low-angle dislocation cells to change into high-angle dislocation cells. It is improbable that multislip would result in dislocation development step by step with the cyclic strain controlled at $\Delta\varepsilon/2 = 0.2\%$ according to this study as multislip caused the primary and secondary hardening to merge into one.

It is worth noting that fatigue failure inevitably occurs in a fatigued process with secondary hardening or with sharp primary (rapid) hardening. There are two types of the cell structures considered in this study, which we distinguish with sizes smaller or larger than 2 μm, and define them as small dislocation cells and large dislocation cells, respectively, for the following reasons. Some studies of crack propagation in BCC metals have pointed out that the dislocation cells always form in front of a crack tip and near the side of the crack [34–36]. Awatani et al. [34] have indicated that the dislocation cell size apparently decreases with any decrease in the distance from the crack. This

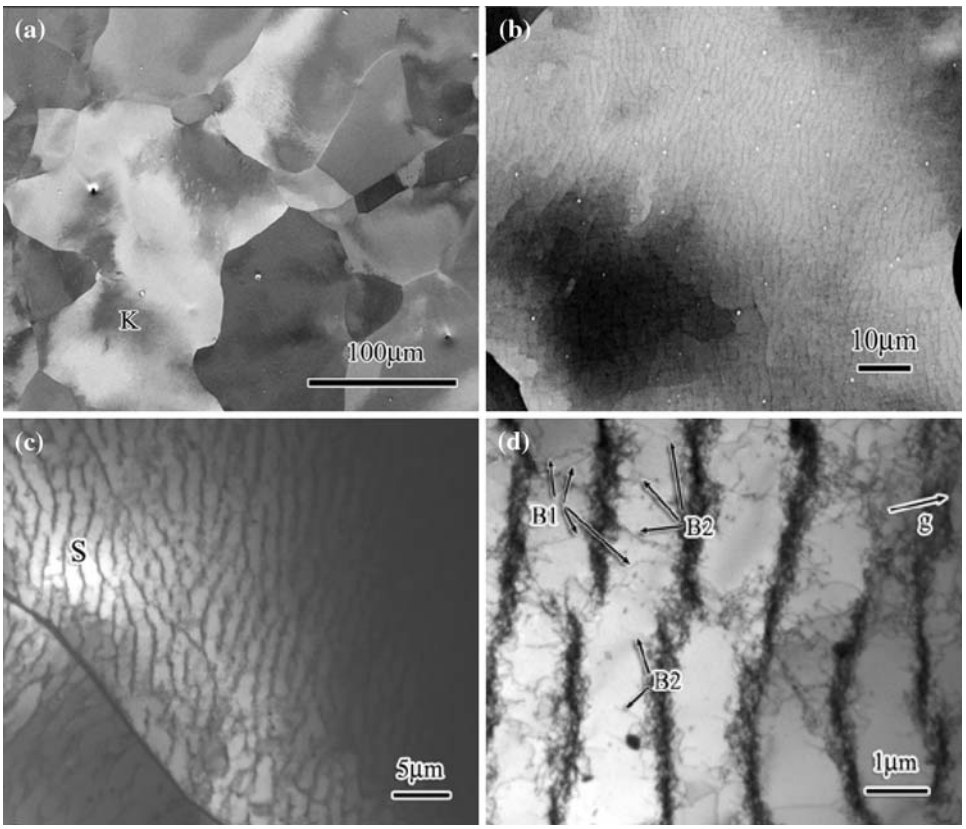

Fig. 5 Microstructure of IF steel cyclically deformed at $\Delta\varepsilon/2 = 0.2\%$ and cycled to 500 cycles without failure (sample J2): **a** SEM micrograph under BEI/ECCI mode showing no contrast within the grains, this represents there is no misorientation in all grains; **b** mark R in (**a**) revealed detail dislocation wall structure; **c** similar morphologies shown in TEM/BFI for comparison; and **d** mark S in (**c**) showing many dislocations of different two Burgers vectors are gliding in the channels of the dislocation wall structure where $B \approx [111]$, $g = [1-10]$

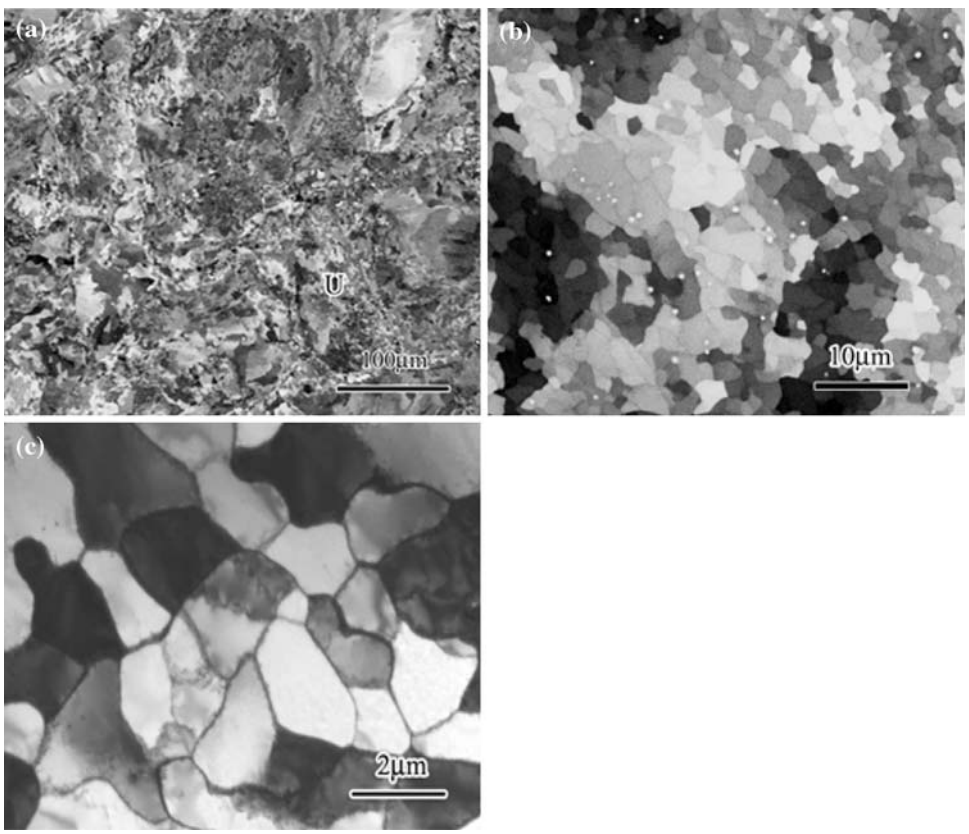

Fig. 6 Microstructure of IF steel cyclically deformed at $\Delta\varepsilon/2 = 0.2\%$ and cycled to failure (sample J3): **a** SEM micrograph observation under BEI/ECCI mode showing high-angle dislocation cells predominate in the dislocation structure due to contrastive divergence inside the grains; **b** mark U in (**a**) revealed detail dislocation cell structure; and **c** similar morphologies shown in TEM/BFI for comparison

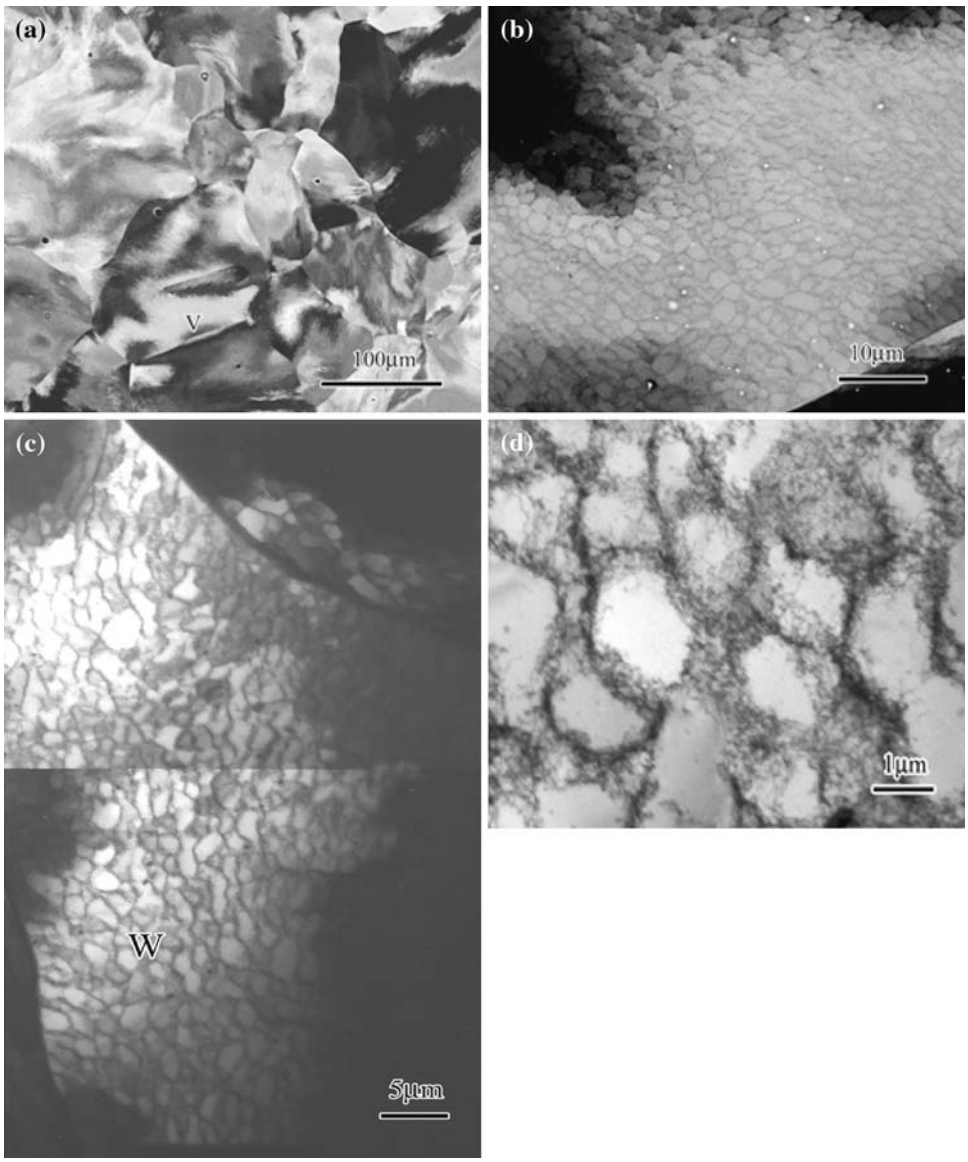

Fig. 7 Microstructure of IF steel cyclically deformed at $\Delta\varepsilon/2 = 1.0\%$ and cycled to 30 cycles without failure (sample K1): **a** SEM micrograph under BEI/ECCI mode showing no severe contrast within the grains, this represents there is no obvious misorientation within all grains; **b** mark V in (**a**) showing the low-angle dislocation cells; **c** similar morphologies shown in TEM/BFI for comparison; and **d** mark W in (**c**) showing the detail dislocation cells with low-angle misorientation

suggests that the smaller dislocation cells near the crack are unable to develop anymore, allowing the fatigued crack with a higher stress intensity factor tends to penetrate the smaller dislocation cells. As a result, these smaller dislocation cells momentarily provide the driving force for crack growth, whereas the larger dislocation cells cannot. The small dislocation cells observed in this study are truly saturated and cannot develop anymore as suggested by the above literature. Thus the dislocation gliding inside the small dislocation cells will be restricted effectively, which results in hardening, and, finally, fatigue failure. The forming of a small dislocation cell structure in this experiment only occurs when the cyclic hardening curve exhibits a sharp primary hardening ($\Delta\varepsilon/2 = 1.0\%$) or when the cyclic hardening curve exhibits a secondary hardening ($\Delta\varepsilon/2 = 0.2\%$). The formation also occurs in a negligible number of cases when the strain amplitude is controlled at $\Delta\varepsilon/2 = 0.1\%$. Therefore, the formation of small dislocation cells indicates the onset of cyclic hardening and fatigue failure. By contrast, fatigue failure will not occur if the strain amplitude is controlled at $\Delta\varepsilon/2 = 0.1\%$, under which the cyclic hardening curve exhibits no obvious primary and secondary hardening. We believe this is because the large dislocation cells are just too large in size. Thus the large dislocation cells cannot restrain the dislocation gliding effectively, hence not having any significant effect on the cyclic hardening curve. Therefore, we can distinguish small dislocation cells from their large counterparts by whether they can provide cyclic hardening or not. We demonstrate that the occurrence of fatigue failure is inevitably accompanied by the formation of small dislocation cells, whereas the large dislocation cells have no significant effect on cyclic hardening nor on the occurrence of fatigue failure.

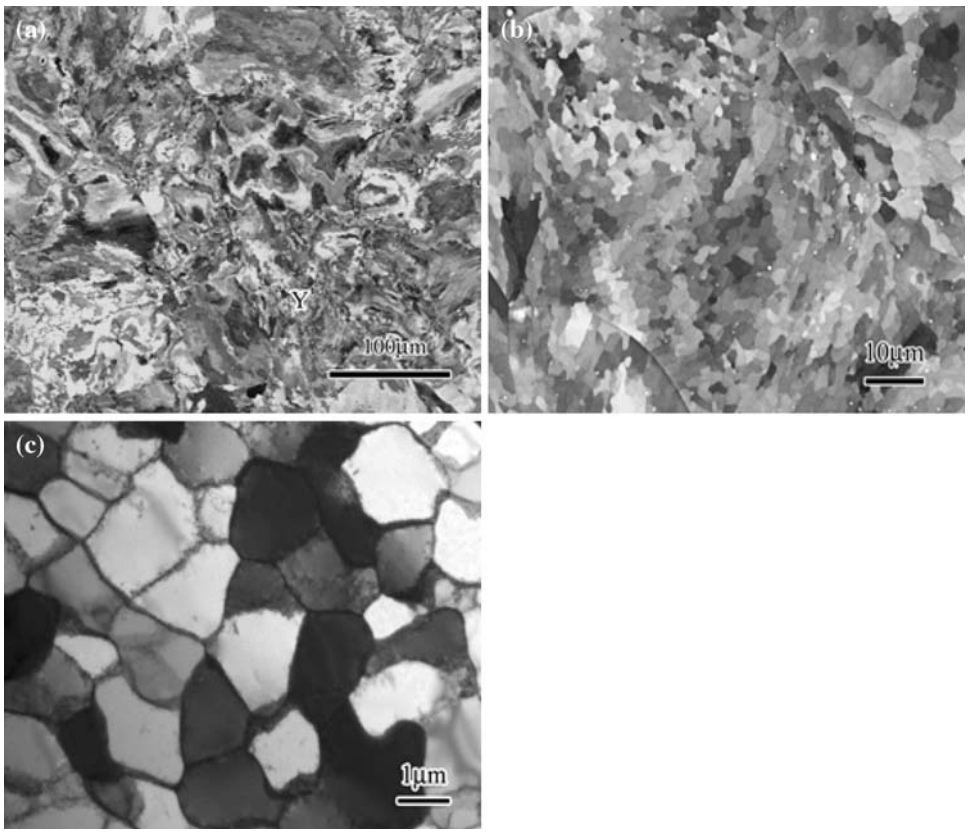

Fig. 8 Microstructure of IF steel cyclically deformed at $\Delta\varepsilon/2 = 1.0\%$ and cycled to failure (sample K2): **a** SEM micrograph observation under BEI/ECCI mode showing high-angle dislocation cells predominate in the dislocation structure due to contrastive divergence inside the grains; **b** mark Y in (**a**) revealed detail dislocation cell structure; and **c** similar morphologies shown in TEM/BFI for comparison

Conclusions

1. There are three types of hardening curves for cyclically deformed IF steel in this study and they show a dependence of strain amplitude as follows:
   (a) $\Delta\varepsilon/2 = 0.1\%$: there is no apparent occurrence of cyclic hardening.
   (b) $\Delta\varepsilon/2 = 0.2\%$: secondary cyclic hardening takes place prior to fatigue failure.
   (c) $\Delta\varepsilon/2 = 1.0\%$: there is only an initial rapid-hardening stage.
2. In this study, we distinguish the small dislocation cells from large dislocation cells by identifying which are smaller or larger than 2 μm and whether they can provide cyclic hardening or not.
3. The gliding behavior of dislocations for $\Delta\varepsilon/2 = 0.1\%$ from early stage to 4×10^5 cycles is a single slip principally, hence the loop patches/veins were mainly composed of primary Burgers vectors.
4. For $\Delta\varepsilon/2 = 0.2\%$, the general dislocation structure prior to secondary hardening predominantly exhibits a dislocation wall structure, whereas the forming of dislocation cells is accompanied by a secondary cyclic hardening. These dislocation walls comprise two kinds of Burgers vector, showing that two Burgers vectors can start simultaneously in the early stage of cyclic deformation, which can be treated as double slip.
5. The low-angle dislocation cells originating from multislip are formed in the early stage of cyclic deformation when the strain amplitude is controlled at $\Delta\varepsilon/2 = 1.0\%$. The low-angle cells are gradually converted into high-angle dislocation cells by the accumulation of cyclic strain.

Acknowledgements This research was supported by the National Science Council, Taiwan, ROC under contract NSC94-2216-E-110-008, and partly by the Center for Nanoscience and Nanotechnology at National Sun Yat-Sen University.

References

1. Luoh T, Chang CP (1998) Mater Sci Eng A256:18
2. Toribio J, Kharin V (2006) J Mater Sci 41:6015. doi: 10.1007/s10853-006-0364-5
3. Kuokkala VT, Kettunen P (1985) Acta Metall 33:2041
4. Polák J, Obrtlík K, Hájek M, Vašek A (1992) Mater Sci Eng A151:19
5. Magnin T, Ramade C, Lepinoux J, Kubin LP (1989) Mater Sci Eng A118:41
6. Wang R, Mugrhabi H (1984) Mater Sci Eng 63:147
7. Gerland M, Violan P (1986) Mater Sci Eng 84:23
8. Chen CY, Huang JY, Yeh JJ (2003) J Mater Sci 38:817. doi: 10.1023/A:1021817216519

9. Wang R, Mugrhabi H, McGovern S, Rapp M (1984) Mater Sci Eng 65:219
10. Figueroa JC, Bhat SP, Delaveaux R, Murzenski S, Laird C (1981) Acta Metall 29:1667
11. Fujii T, Shintate H, Yaguchi H, Mitani H, Inada A, Shinkai K, Kumai S, Kato M (1997) ISIJ Int 37:1230
12. Videm M, Ryum N (1996) Mater Sci Eng A219:1
13. Videm M, Ryum N (1996) Mater Sci Eng A219:11
14. Lin TL, Wu JS, Chen XF (1987) Mater Sci Eng 86:19
15. Planell JA, Guiu F (1986) Philos Mag A54:325
16. Mori H, Tokuwame M, Miyazaki T (1979) Philos Mag A40:409
17. Mori H, Oba N, Miyazaki T, Kozakai T (1980) Philos Mag A42:483
18. Šesták B, Novák V, Libovický S (1988) Philos Mag A57:353
19. Mughrabi H, Herz K, Stark X (1981) Int J Fract 17:193
20. Mughrabi H, Herz K, Stark X (1976) Acta Metall 24:659
21. Sommer C, Mughrabi H, Lochner D (1998) Acta Metall 46:1527
22. Abdel-Raouf H, Plumtree A (1971) Metall Trans 2:1863
23. Chopra OK, Gowda CVB (1974) Philos Mag 30:583
24. Ikeda S (1981) Trans Jpn Inst Met 22:267
25. Kuhlmann-Wilsdorf D, van der Merwe JH (1982) Mater Sci Eng 55:79
26. Kuhlmann-Wilsdorf D (1987) Mater Sci Eng 86:53
27. Li XW, Zhou Y (2007) J Mater Sci 42:4716. doi:10.1007/s10853-007-1758-8
28. Ahmed J, Wilkinson AJ, Roberts SG (2001) Philos Mag A81:1473
29. Ahmed J, Wilkinson AJ, Roberts SG (1997) Philos Mag Lett 76:237
30. Li SX, Li MY, Zhu R, Chao YS (2004) Philos Mag 84:3323
31. Huang HL, Ho NJ (2003) Mater Sci Eng A345:215
32. Huang HL, Ho NJ (2000) Mater Sci Eng A279:254
33. Kaneko Y, Ishikawa M, Hashimoto S (2005) Mater Sci Eng A400–401:418
34. Awatani J, Katagiri K, Nakai H (1978) Metall Trans 9A:111
35. Ogura T, Masumoto T (1976) Trans Jpn Inst Met 17:733
36. Awatani J, Katagiri K, Shiraishi T (1976) Metal Trans 7A:807